

MEMS Accelerometer Mini-Array (MAMA): A Low-Cost Implementation for Earthquake Early Warning Enhancement

Ran N. Nof,^{a),b)} Angela I. Chung,^{a)} Horst Rademacher,^{a)} Lori Dengler,^{c)} and Richard M. Allen^{a)}

Earthquake Early Warning Systems (EWS) are often challenged when the earthquakes occur outside the seismic network or where the station density is sparse. In these situations, poor locations and large alert delays are more common because of the limited azimuthal coverage and the time required for the wavefield to reach the minimum number of seismic stations to issue an alert. Seismic arrays can be used to derive the directivity of the wavefield and obtain better location. However, they are uncommon because of the prohibitive cost of the sensors. Here, we propose the development of an array-based approach using mini-arrays of low-cost Microelectromechanical Systems (MEMS) accelerometers and show how they can be used to improve EWS. In this paper, we demonstrate this approach using data from two MEMS Accelerometer Mini-Arrays (MAMA) deployed at University of California Berkeley and Humboldt State University. We use a new low-cost (<U.S. \$150) Data Acquisition Unit and solve for the back azimuth of seven events with magnitudes ranging from Mw 2.7 to 5.1 at distances of 5 km to 106 km. [DOI: 10.1193/021218EQS036M]

INTRODUCTION

A significant problem faced by Earthquake Early Warning Systems (EWS) is the correct characterization of earthquakes that occur at either the edge of or outside of the seismic network. Because of poor azimuthal coverage, location estimate errors can be considerable (Figure 1). The median location error for earthquakes occurring outside of the Northern California EEW seismic network for $M \geq 4$ events between 1 February 2016 and September 11, 2017, detected by the ElarmS EWS (Kuyuk et al. 2014) is 44.4 km, with a standard deviation of 49.9 km. In contrast, the median location error for all $M \geq 4$ events that occurred within the Northern and Southern California networks during the same time period is just 4.0 km, with a standard deviation of 26.5 km. Without accurate location estimates, EWS cannot correctly estimate ground shaking, and they are then unable to deliver timely alerts to affected areas.

Seismic arrays have been used for nuclear test monitoring and seismological research since the 1960s (e.g., Birtill and Whiteway 1965). They are commonly used to obtain the slowness vector of the wavefield and to increase signal-to-noise ratio (SNR). Despite

^{a)} Berkeley Seismology Lab, University of California Berkeley, Berkeley, CA 94703; Email: ran.nof@gmail.com (R. N. N.)

^{b)} Geological Survey of Israel, Jerusalem, Israel 9550161

^{c)} Geology Department, Humboldt State University, Arcata, CA 95521

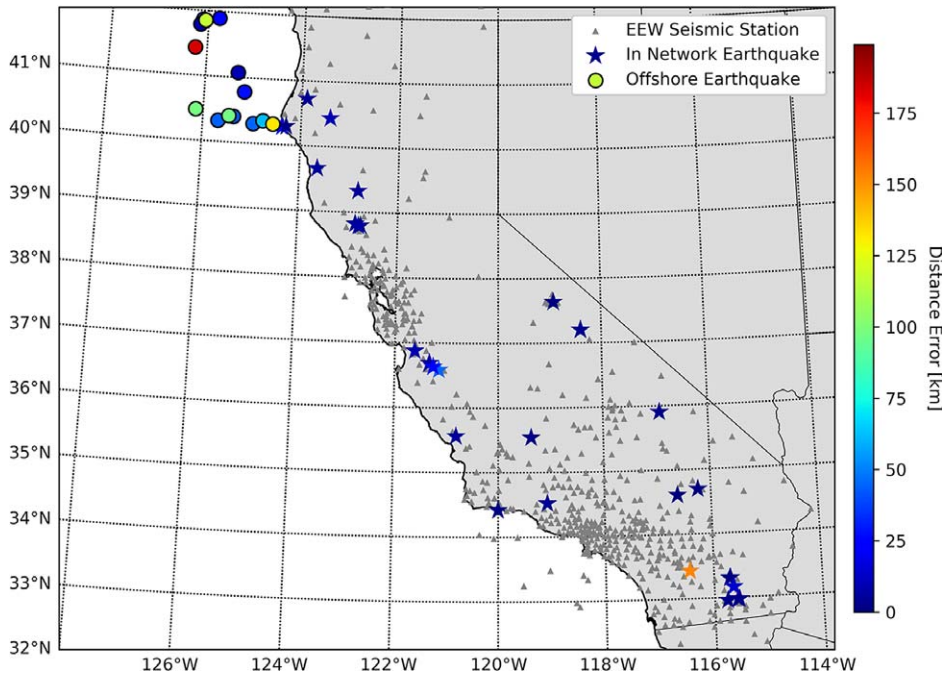


Figure 1. Map of $M \geq 4$ earthquakes occurring within (stars) or outside of (circles) California EEW seismic network (triangles) between 1 February 2016 and September 11, 2017, and detected by ElarmsS, colored by distance error from the ANSS catalog locations. Note that there is one event in Southern California on 10 June 2016 with a distance error of 153 km because of some traces picking on the S-wave. Without this event, the median distance error is 3.9 km, with a standard deviation of 9.0 km for earthquakes within the network.

the obvious advantages over regular seismic networks, seismic arrays are not very common worldwide. One reason they are not frequently used is the high cost of augmenting each network station with further conventional seismic sensors to give it array functionality. Here, we describe the development of an array-based approach using low-cost Microelectromechanical Systems (MEMS) accelerometers.

MEMS capacitive accelerometers are devices with a very small footprint (micrometers to a few millimeters in size) and with low power consumption. They are capable of measuring relative gravitational changes (Middlemiss et al. 2015). MEMS have been used in seismology since the beginning of the millennium (Holland 2003). Recently, several attempts were made to include class-C [Advanced National Seismic System (ANSS) 2008] low-cost MEMS accelerometers in seismological investigations, mainly by using dense networks of such sensors (e.g., Clayton et al. 2015). The individual instruments can be attached to volunteers' computers (e.g., Cochran et al. 2009), or they can be installed as independent instruments at individual hosts (e.g., Clayton et al. 2011) or in public buildings such as schools, hospitals, and places of worship (e.g., D'Alessandro 2014). Another approach is to exploit a network of built-in MEMS sensors in smartphones (Finazzi 2016, Kong et al. 2016).

Low-cost MEMS sensors have also been used to rapidly create seismic networks, monitoring aftershock seismic activity following large events (e.g., [Chung et al. 2011](#), [Lawrence et al. 2014](#)). Because of their low price, low power, and small size, a large number of devices can be deployed in a short time. Another use of MEMS accelerometers in seismological research is to combine them with single-channel GPS devices to resolve baseline errors ([Minson et al. 2015](#), [Tu et al. 2013](#)). The development of an earthquake early warning alerting device based on a MEMS sensor and a 10-bit digitizer has also been proposed (e.g., [Zheng et al. 2011](#)).

It is clear that these low-cost MEMS sensors with maximum resolutions of 16 bits are capable of detecting moderate to large earthquakes at distances of several tens of kilometers away ([D’Alessandro and D’Anna 2013](#), [Evans et al. 2014](#), [Yildirim et al. 2015](#)). With their growth in popularity and commercial potential in many research fields, the sensitivity of MEMS devices has significantly improved over time. For instance, between 2011 and 2013, the noise level of smartphone MEMS was reduced by ~ 20 dB at the bandwidth of 1–10 Hz ([Kong et al. 2016](#)). Some new MEMS accelerometers currently being tested have low noise floors of up to $2 \text{ ng}/\sqrt{\text{Hz}}$ ([Pike et al. 2014](#)), while others have wider bandwidth (as low as 10^{-4} Hz) and higher resolution based on resonance technology ([Middlemiss et al. 2015](#), [Zou et al. 2014](#)). These improvements led to the use of class-B sensors in EEWs in Japan and Taiwan ([Horiuchi et al. 2009](#), [Wu 2015](#)).

Available off-the-shelf class-C sensors are, however, limited to digital sensors with resolutions of 16 bits or less or to analog sensors that require additional analog-to-digital converter (ADC) units. In the following, we first describe our rationale for building a MEMS Accelerometer Mini-Array (MAMA) and demonstrate its use to estimate the back azimuth (BAZ) of local earthquakes. The array uses a new specially designed data acquisition unit (DAU), which is a single device with integrated class-C MEMS sensor, 24-bit digitizer, and data logger. Finally, we discuss how the application of MAMA can enhance EEWs.

MAMA DESIGN

In order to mitigate the high cost of installing a seismic array using conventional seismometers, we propose the use of multiple low-cost MEMS accelerometer DAUs. They will be arranged as a MAMA with a small aperture of 200–1,000 m, preferably around an existing conventional seismometer or strong-motion sensor where available. Ideally, one of the DAUs should be colocated with the existing instrument. Such a layout is designed to improve the recordings of a single conventional network station by employing well-known array methods whenever the epicentral distance is much greater (at least 10-times larger) than the array aperture. For its power and telemetry needs, each DAU in the mini-array can draw from the already available resources of the conventional station at remote locations or simply be connected to dedicated power and Wi-Fi where available. Colocating one of the DAUs with the conventional seismic instrument will further constrain the possible time shifts between the time controllers of the traditional network and the MEMS DAU, which most likely will be using Network Time Protocol. It can also be used for other quality control evaluations based on the comparison of waveforms.

The major limitation of using a MAMA is the high intrinsic noise and low sensitivity of currently available class-C low-cost MEMS sensors. Though these devices are still usable for analyzing large magnitude earthquakes or moderate earthquakes at shorter distances,

the lower quality of these devices limits the magnitude detection threshold (Evans et al. 2014). Some examples of possible uses of MAMAs include calculating BAZ based on the arrival times at each node or solving for the slowness vector of a wave field or its propagation pattern within the array. For large magnitude earthquakes, where the rupture propagates along longer fault traces, back-projecting the source location would make it possible to investigate fault dimensions (Fletcher et al. 2006, Meng et al. 2014, Spudich and Crowswick 1984). The method of back-projecting is commonly used at teleseismic distances and low frequencies. Given the lower sensitivity of the MEMS and limited bandwidth, our approach is to use MAMA for BAZ or back-projection at local distances and high frequencies of 1–10 Hz (Allmann and Shearer 2007). In the following, we describe our new DAU device, deployment, and processing scheme.

MAMA DAU

Currently used off-the-shelf digital class-C MEMS accelerometers are limited to 16-bit resolution with root mean square noise levels down to $45 \mu\text{g}/\sqrt{\text{Hz}}$ (Evans et al. 2014). For a full scale $\pm 2\text{-g}$ sensor, the 16-bit digitizer creates a maximum resolution (minimal single-bit value) of $61 \mu\text{g}/\text{count}$, provided the self-noise of the sensor is lower. In addition, off-the-shelf sensors need to be connected to a computer or a data logger with appropriate code to make the data available for further processing on site or at a remote data center (e.g., Clayton et al. 2015). We have developed a new low-cost (<U.S. \$150) DAU (hereafter referred to as a MAMA node). This unit consists of a printed circuit board (PCB) bearing four analog MEMS accelerometers ($\pm 2\text{-g}$ range) and a 24-bit ADC, and it is combined with a RaspberryPi single-board computer. The RaspberryPi serves as a data logger and is capable of providing online access to the 100 samples-per-second data streams via an onboard seedlink server (for more technical details about the MAMA node, see online Appendix A).

The MAMA node sensor's self-noise level of $50 \mu\text{g}/\sqrt{\text{Hz}}$ is at the lower end of the noise range of most currently available off-the-shelf devices (Evans et al. 2014). In the current version of MAMA node (Revision 0.3), we use four MEMS sensors in parallel to reduce the noise by half and provide improvement of more than 15 dB over off-the-shelf digital accelerometers. Figure 2 shows the MAMA node's mean power spectral density (PSD; McNamara and Buland 2004) for a 1-day period measured at the Berkeley Byerly Vault, which also houses the conventional seismic station BKS Episensor. We also measured the well-tested Quake Catcher Network sensor O-Navi B (Evans et al. 2014) by replacing the PCB on our MAMA node with the O-Navi B sensor and adjusting the code appropriately. For our frequency band of interest of 1 to 10 Hz, the mean PSD levels are -73 to -80 dB ($0.22 \times 10^{-3} - 0.1 \times 10^{-3} \text{ m}^2\text{s}^{-4}/\text{Hz}$), respectively (colored lines, Figure 2). This improvement, though still noisier than class-A strong-motion devices with noise levels lower than -120 dB, significantly improves our capability to obtain useful signals of small magnitude events and allows us to test our approach without needing significant events to occur in the MAMA vicinity. Figure 3 shows a comparison between traces of a Güralp 5TC accelerometer, a MAMA node, and an O-Navi B sensor placed at the Berkeley Byerly Vault for a Mw 3.8 at 40 km event. This figure demonstrates the improved sensitivity of the MAMA node over the O-Navi B, which is one of the highest grade 16-bit sensors available (Evans et al. 2014), as well as its compatibility with a high-end standard force-balance strong-motion sensor where the signal is above its noise levels.

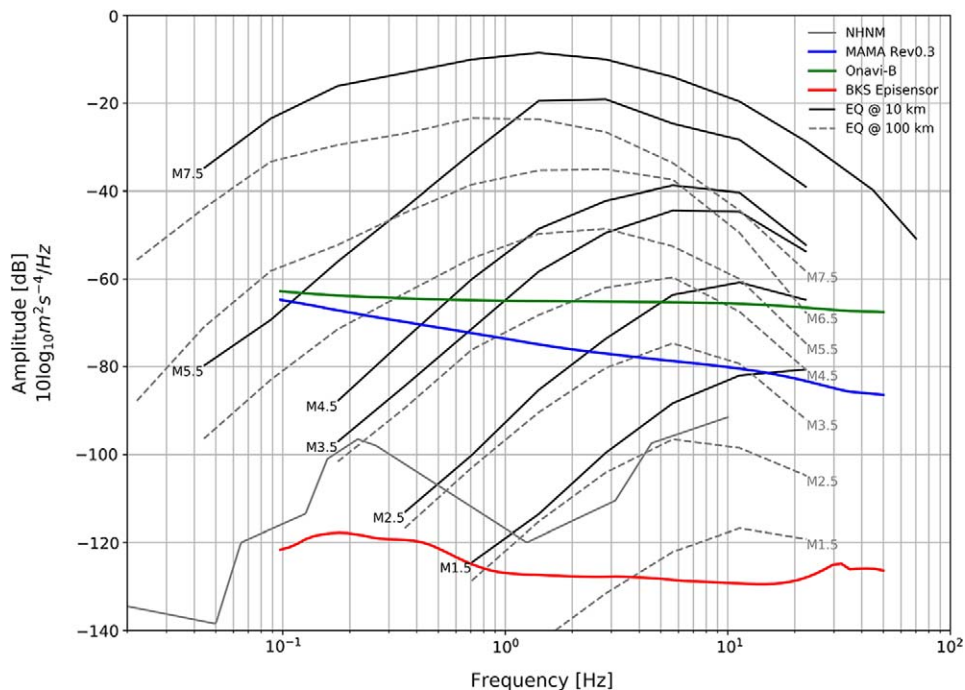


Figure 2. Mean PSD (McNamara and Buland 2004) of a representative MAMA node (MAMA Rev 0.3, blue line) and Quake Catcher Network’s O-Navi B 16-bit MEMS sensor (O-Navi B, green line) installed at the Berkeley Byerly Vault. The conventional strong motion sensor (Episensor) of the BK network located at the Byerly Vault is marked as a red line (BKS station) for comparison of background noise levels. Lines are the mean PSD of the horizontal traces, between 1 September 2016 and 5 September 2016. Earthquake representative spectra responses are marked as dark solid and dashed gray lines for near and far fields, respectively (Clinton and Heaton 2002). New High Noise Model (Peterson 1993) is marked as a solid gray line. Earthquake data converted to dB following Cauzzi and Clinton (2013).

MAMA DEPLOYMENT

We deployed two MAMA arrays (Figure 4a). The first, BRK MAMA, is at the University of California Berkeley campus and is composed of nine nodes around the seismic station (BK.BRK) in Havilland Hall. The maximum distance between two MAMA nodes is 1,200 m (Figure 4b). We placed the MAMA nodes in basement or ground floor offices or in utility rooms. Each node was connected to a wall outlet for power and attached to the floor (aligned to magnetic north using a compass) with a two-sided tape. We note that using this method with the coupling to the ground is not ideal, but it is a very rapid, low-cost, and nonintrusive method suitable for offices and occupied urban areas. Communication with the nodes is done via Wi-Fi or Ethernet. The BRK MAMA was partly operational at the end of December 2016 and was fully deployed in May 2017.

The second MAMA setup is the Accessible Resources Center (ARC) MAMA at the Humboldt State University campus. This array is composed of 13 nodes at nine locations

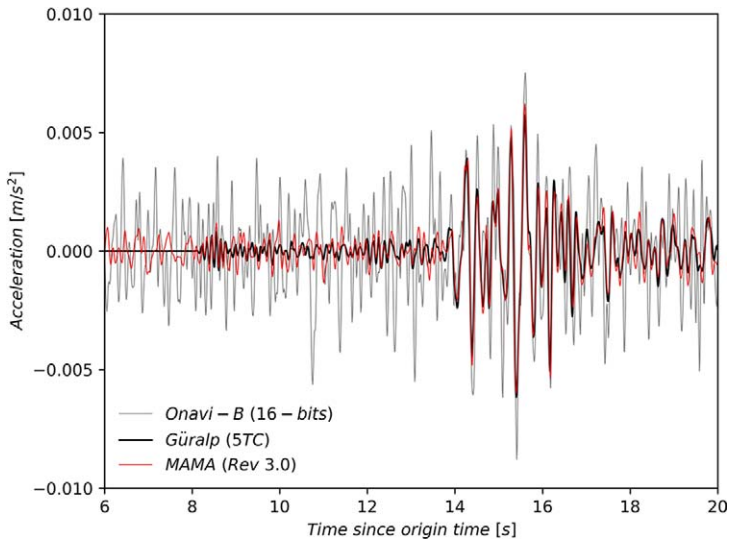


Figure 3. Comparison of north component from a MAMA node device (red), a Güralp 5TC accelerometer (black), and an O-Navi B device (gray) for event nc72795746, an Mw 3.78 located 40.2 km away. All devices were collocated at Berkeley Byerly Vault. Time is relative to origin time. Traces are bandpass filtered between 1 and 10 Hz.

(2 nodes are collocated at four locations). No standard station is available at this site. The maximum distance between two nodes of this MAMA is 845 m (Figure 4c). All sensors are located at utility rooms and communicate over Ethernet. ARC MAMA has been fully operational since 9 March 2017.

Both BRK and ARC MAMA are located within the campuses where power and communication are conveniently available, and MAMA node installations at utility rooms or offices are straightforward and secured. BRK MAMA is in close proximity to the Hayward Fault with the highest earthquake probability in the Bay Area (Field et al. 2017), and ARC MAMA is located close to the Mendocino Triple Junction, one of the most seismically active regions along the San Andreas fault system and where the seismic network is sparse. MAMA node locations are based on the availability of suitable locations across the campuses.

USING MAMA TO SOLVE FOR BAZ

A seismic array consists of numerous seismic instruments located within a relatively close range of one another. Depending on the spacing of the sensors and the wavelength of the signal, a wavefield passing through the array may show a coherent signal. It is also possible to observe the difference in arrival times of the wavefield at each of the instruments. Coherency and arrival time offsets can be used to increase the SNR of a recording and to derive the slowness vector. This can provide the directivity of the wavefield signal. For more details on seismic arrays, see Harjes and Henger (1973), Rost and Thomas (2002, 2009), Schweitzer et al. (2011), and the references therein. Here, we concentrate on using the array capability to calculate BAZ in order to improve the EEWs earthquake location.

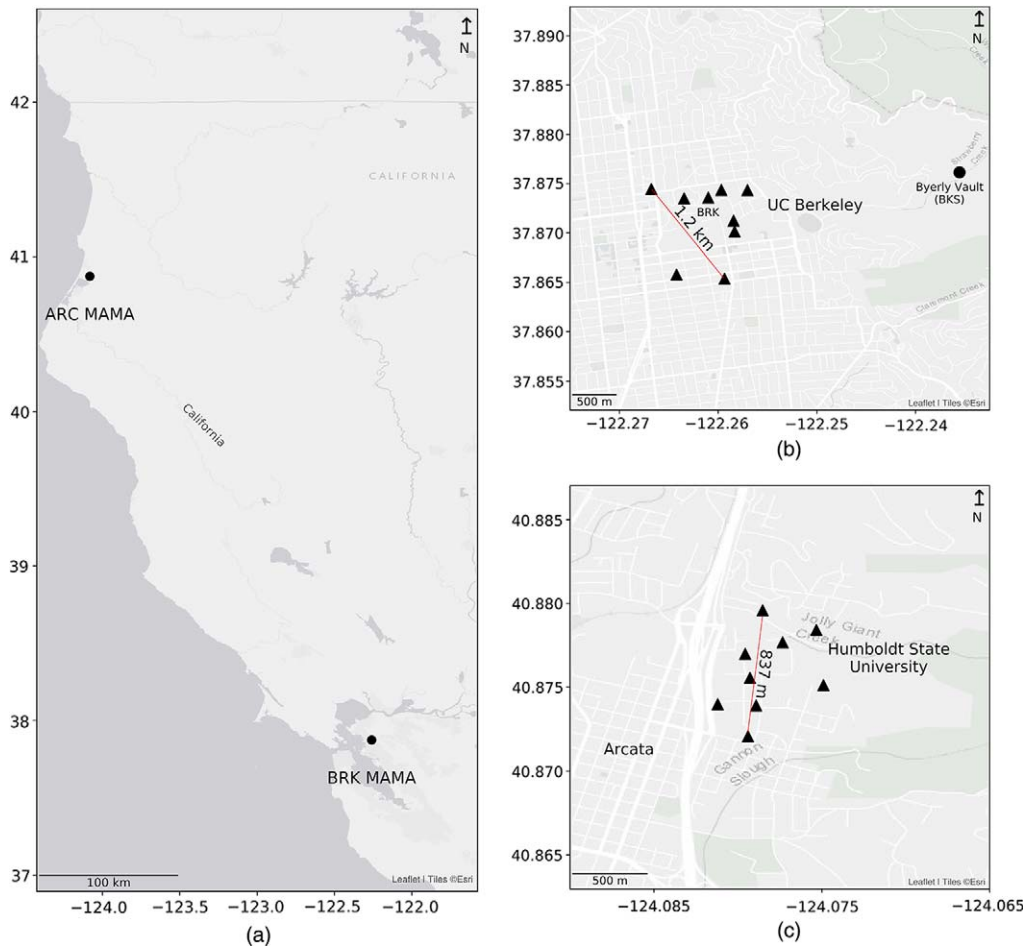


Figure 4. MAMA location map. (a) General location map. (b) BRK MAMA at University of California Berkeley campus, Berkeley, CA. BRK marks the location of the conventional BK. BRK station at Haviland Hall. (c) ARC MAMA at Humboldt State University campus, Arcata, CA. MAMA nodes are marked as triangles.

To calculate the BAZ, we used the freely available ObsPy (Beyreuther et al. 2010) FK analysis tool. This tool uses frequency domain beamforming (i.e., Conventional or Bartlett beamformer) to find the maximum of the power of the beam given different slowness vectors (Bartlett 1950, Harjes and Henger 1973, Nawab et al. 1985). For each event, we calculate the maximum power, normalized by the signal covariance (relative power) and the corresponding BAZ and slowness using 1-s windows with 0.05-s steps.

Though we are aiming at developing a real-time processing module, we currently use an automated off-line processing scheme. While the real-time module should have its own earthquake identifier, the current code is regularly querying USGS's ANSS Catalog (see data and resources section) for events of $M_w > 2.5$ up to a 110-km radius from the MAMA center.

We automatically process the waveforms from the MAMA nodes and the standard seismic station as available, beginning 20 s before and ending 40 s after the origin time of the event. We use a simple STA/LTA triggering detector to identify the event arrival if more than 40% of all traces (two horizontals and one vertical for each node) have triggered with SNR above 5. Once an event is labeled as “Identified,” the BAZ is then calculated using the following steps:

1. Detrend, removing a mean value.
2. Bandpass using a Butterworth filter at 1–10 Hz.
3. Remove gain value, converting to m/s^2 units.
4. Obtain a representative trace tr for each node from the three components. This is to mitigate misaligned nodes:

$$tr = \sqrt{N^2 + E^2 + Z^2} \cdot \text{sign}(Z) \quad (1)$$

where N , E , and U are the North, East and Z traces of the node, respectively. All following processing is done on the representative trace tr .

5. Use a simple STA/LTA trigger to detect first arrival time to the MAMA. Calculate the Cumulative Cross-Correlation values (CCC) for each node using the following equations:

$$CCC_i = \sum_{j \neq i}^n cc_{ij} \quad (2)$$

$$cc_{ij} = \frac{\sum tr_i \cdot tr_j}{\sqrt{\sum tr_i^2 \cdot \sum tr_j^2}} \quad (3)$$

where i indicates a node, and j iterates over the rest of the n nodes.

6. Where collocated nodes exist, discard the one with lower CCC values.
7. If $CCC < \text{mean}(CCC) - 1.5 \cdot \sigma(CCC)$, then discard the trace with the lowest CCC , recalculate CCC , and repeat discarding until a minimum of four traces are left or no trace has such a low CCC value. This step helps to mitigate strong site effects and poorly coupled nodes.
8. BAZ process for a span of 2 s before the first trigger and 20 s after. Processing is done using a sliding window of 1 s and a 0.05-s step.
9. The processing results for each window are the maximal relative power of the array, BAZ, and slowness. We derive the mean BAZ of all windows where relative power is within the top 15% along the processing span and the slowness is below one to exclude non-body wave signals and maintain relatively high coherence values.

RESULTS

Using the automatic processing scheme described above, between 9 March 2017 and 1 August 2017, 4 out of 23 events were identified by the BRK MAMA and 6 out of 33 events were identified by the ARC MAMA (Table 1). Of the identified events, we successfully calculate BAZ for three and four events at the BRK and ARC MAMAs, respectively. Figure 5

Table 1. A list of identified ANSS catalog events from all event with magnitude >2.5 and distance less than 110 km from BRK and ARC MAMA

MAMA	ANSS event ID	Origin time	Distance (km)	M	Type	Observed BAZ	Calculated BAZ	BAZ standard deviation	Identified wave-front
ARC	nc72772046	9 March 2017 11:21:07	40.3	2.8	md	151	N/A	N/A	S
BRK	nc72795746	30 April 2017 01:29:19	40.2	3.78	mw	97	95.8	77.3	S
BRK	nc72801976	15 May 2017 22:50:03	21.1	2.72	md	55	49.5	0.6	S
BRK	nc72806646	26 May 2017 07:56:59	19.9	2.52	md	58	N/A	N/A	S
ARC	nc72807961	29 May 2017 19:34:09	66.9	2.62	md	255	N/A	N/A	S
ARC	nc72814101	11 June 2017 12:19:29	18.7	3.53	mw	351	351.6	80.8	P
BRK	nc72819101	21 June 2017 19:00:20	5	3.02	mw	323	323.6	8.6	P
ARC	nc72820761	24 June 2017 21:22:03	67.8	4.03	mw	195	184.6	0.1	S
ARC	nc72852151	29 July 2017 00:02:40	93.6	5.11	mw	264	271.8	2.5	P
ARC	nc72852946	29 July 2017 17:08:26	107.7	4.57	mw	282	273.2	1	P

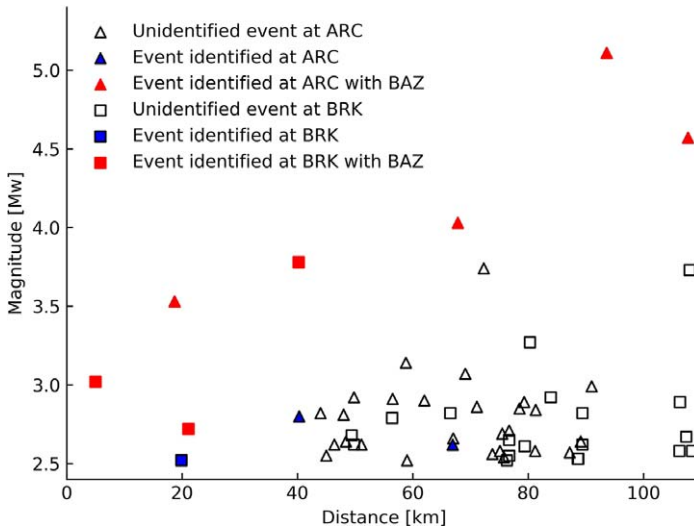


Figure 5. MAMA detection and BAZ calculation performance. All events with $M > 2.5$ and less than 110 km from a MAMA are plotted as triangles and squares for ARC and BRK MAMAs, respectively. Red markers represent identified events with calculated BAZ within 30° of the observed BAZ. Blue markers represent identified events with calculated BAZ more than 30° different from the observed BAZ. Empty markers represent events unidentified by MAMA.

shows the BAZ and event identification threshold with respect to magnitude and distance. With the available data, we are able to calculate BAZ for earthquakes with magnitudes as low as $M_d 2.7$ at 20 km distance.

To illustrate the processing results, we show in Figure 6 the results of the FK analysis of event nc72819101, which occurred on 2017-06-21T19:00:20, with $M_w 3$ at a distance of 5 km from the BRK MAMA. The observed BAZ between the MAMA center and the ANSS catalog location is 323° . The mean calculated BAZ is 323.6° , with a standard deviation of 8.6° . The BAZ was obtained using just 1.8 s of data following the P-wave trigger. Event nc72795746, which occurred on 2017-04-30T01:29:19, with $M_w 3.78$ at 41 km away from the BRK MAMA does not perform as well. The BAZ between the MAMA center and the ANSS catalog location is 95° . Though the mean MAMA-estimated BAZ is 95.8° , which is very close to the observed BAZ, the standard deviation is 77.3° and the BAZ ranges from -9.5° to 162° , as shown in Figure 7. Finally, Figure 8 shows an example of event nc72806646, which occurred on 2017-05-26T07:56:59, with $M_w 2.52$ at 19.9 km away from the BRK MAMA. This event was identified by the automatic triggering, but it failed to obtain BAZ using our current processing scheme because of low SNR. BAZ plots for all the identified events listed in Table 1 are available in the online Appendix B.

DISCUSSION AND OUTLOOK

Comparing the MAMA nodes' mean PSD noise floor with representative earthquake spectral responses (Clinton and Heaton 2002) suggests that the new MAMA node described

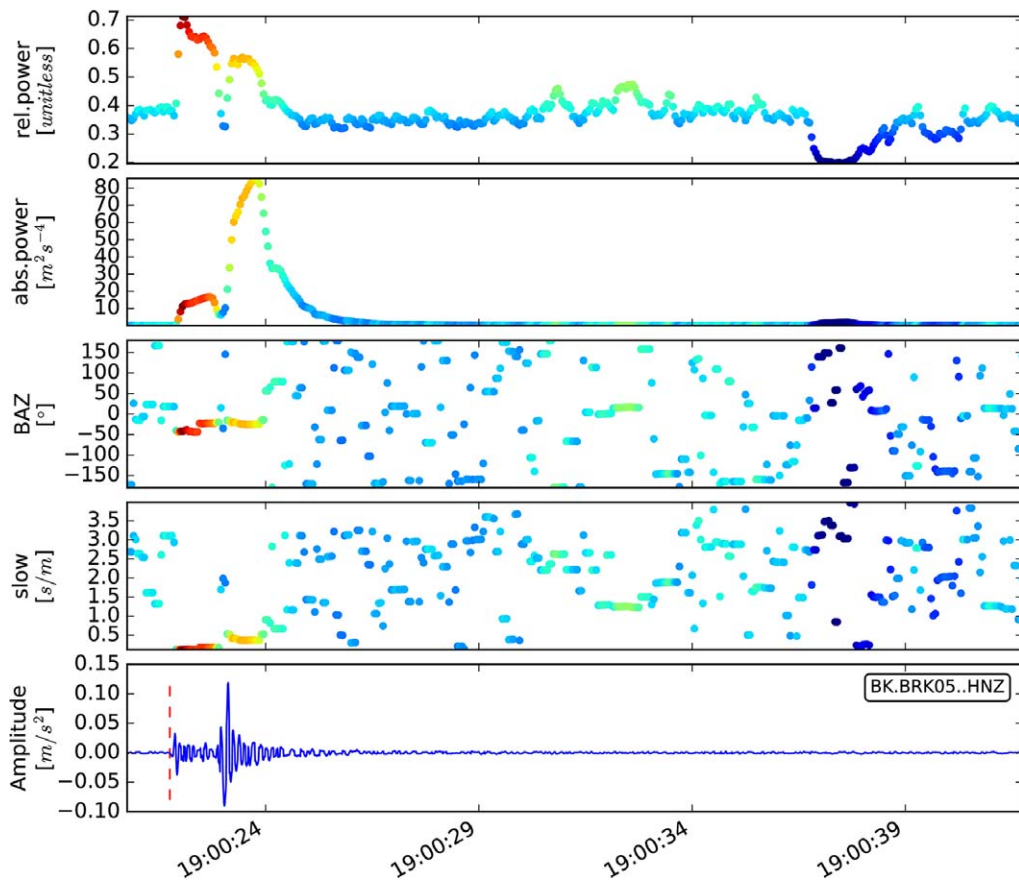


Figure 6. BAZ calculation plot for event nc72819101 2017-06-21T19:00:20, Mw 3, 5 km away from BRK MAMA. Subplots from the top are relative power, absolute power, BAZ, slowness, and a typical MAMA node acceleration waveform with the trigger time marked by a dashed red line. Each point represents the calculations done for a 1-s data window ending at point position along x-axis. Colors represent the amplitude of the relative power values. The observed BAZ between the MAMA center and the ANSS catalog location is 323° . The mean calculated BAZ is 323.6° , with a standard deviation of 8.6° . This result was obtained 1.8 s after the trigger time.

above has the potential to detect peak accelerations of Mw > 2.5 earthquakes at ~ 10 km and Mw > 3.0 at ~ 100 km (Figure 2). Indeed, the current MAMA node (Rev 0.3) was able to detect a Mw 2.5 at 20 km using our automatic processing scheme.

Though our results correspond well to the expected performance of our low-cost DAU, there are some limitations. The low number of events detected, with respect to the number of events at a 100-km range, is a result of the low sensitivity of the sensors and the method's sensitivity to low SNR. This sensitivity limits the number of events available for processing and obtaining BAZ results. Typically for EEW, destructive earthquakes of Mw > 4.5 are of

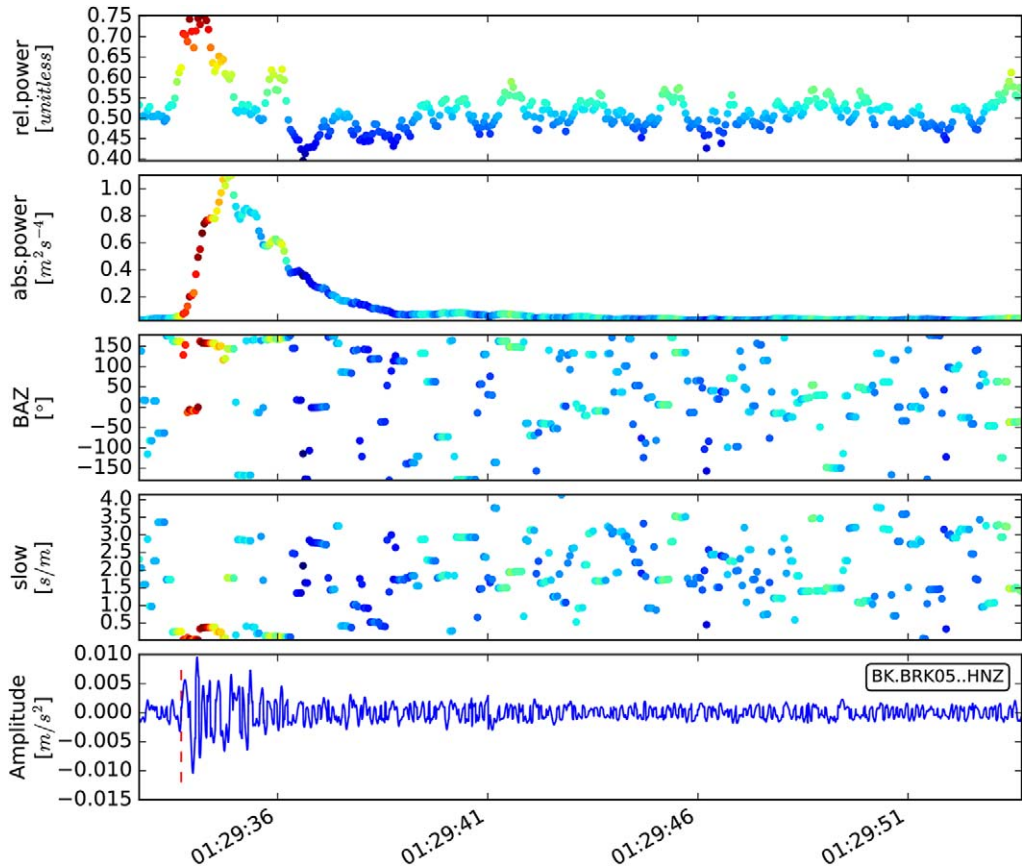


Figure 7. Similar to Figure 6, BAZ calculation plot for event nc72795746 2017-04-30T01:29:19, Mw 3.78, 41 km away from BRK MAMA. The observed BAZ between the MAMA center and the ANSS catalog location is 95° . The mean calculated BAZ is 95.8° , with a standard deviation of 77.3° . The result was obtained 1.65 s after the trigger time.

interest for mitigation actions. However, testing and training the EEWs as well as the public would require a higher rate of events, which may not be available everywhere. For that reason, higher sensitivity is required to be able to obtain BAZ results for lower magnitude events, which are more common.

Our new devices, when arranged in mini-arrays, can be used for improved source characterization that could be particularly important for EEW. As demonstrated, the MAMA can be used to rapidly obtain the BAZ of an event 2–3 s after the arrival of P-waves to the MAMA, depending on the SNR. To illustrate a potential use of MAMA, Figure 9 shows an example of a mislocated Mw 4.5 event on 5 December 2016 near Petrolia, CA. The BAZ from the second station to detect the event, Station NC.KMPB, to the ANSS location is 236° , while the BAZ to the ElarmS location of first alert is 303° . Assuming a MAMA around station NC.KMPB and a 5-s delay to process the data and calculate the BAZ, a better

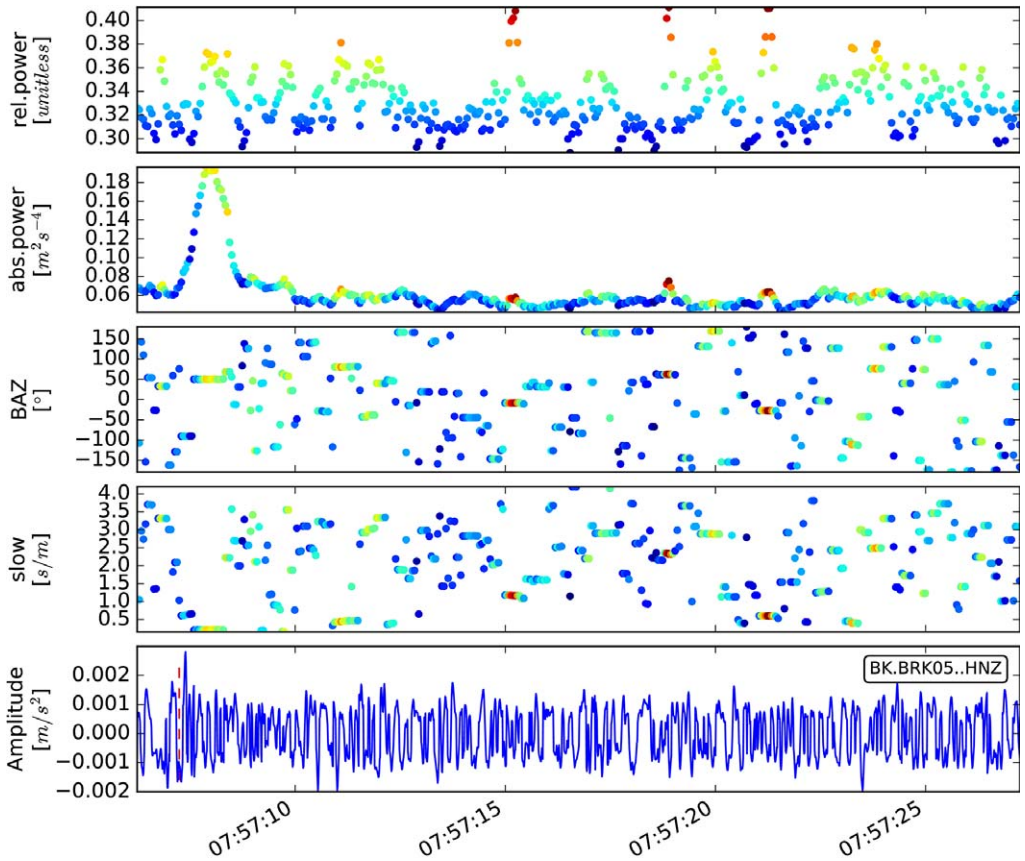


Figure 8. Similar to Figure 6, BAZ calculation plot for event nc72806646 2017-05-26T07:56:59, Mw 2.52, 19.9 km away from BRK MAMA. The observed BAZ between the MAMA center and the ANSS catalog location is 58° . The BAZ could not be calculated because of the low SNR.

location might be achieved without delaying the alert time, which was sent 6 s after P-wave arrival to the station. The large alert time delay is due to an ElarmS requirement that four stations must have detected an event before an alert can be sent out. Combining multiple MAMA may make it possible to robustly estimate the epicenter of an earthquake based on just two arrays instead of the current requirement of four stations. This would decrease the time needed for point source EEWs to issue an alert, especially where the seismic network is sparse.

In addition to providing information about BAZ for point-source earthquakes, the evolution of BAZ information during a large magnitude event can provide more detailed source characterization. Using local high-frequency energy back projection (e.g., Allmann and Shearer 2007, Meng et al. 2014) allows for the estimation of the rupture propagation pattern (speed, duration, directivity, segmentation) and the better estimation of the total rupture

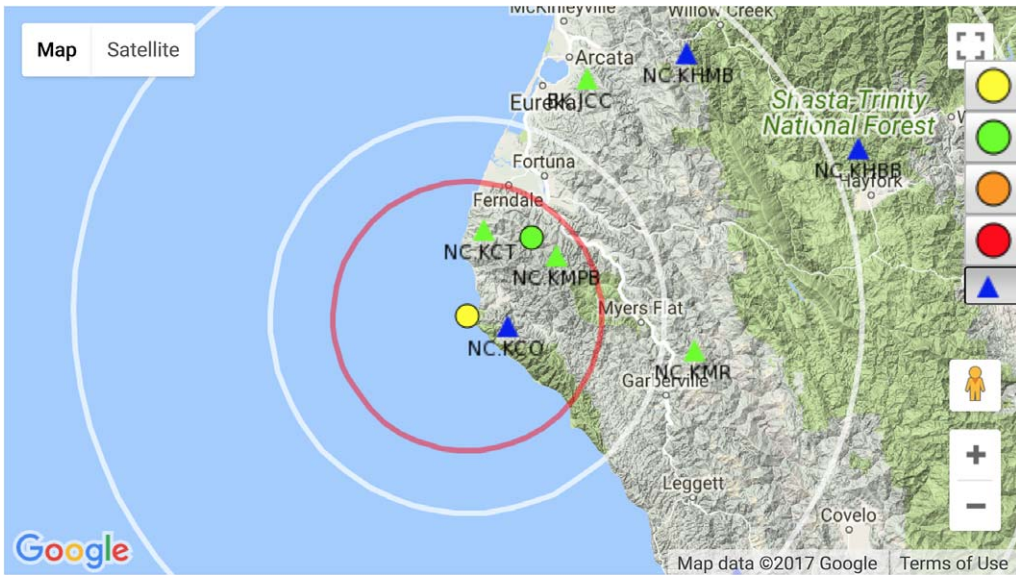


Figure 9. Elarms review tool snapshot of the first alert of Mw 4.5 earthquake that occurred on 5 December 2016 at 18:55. Yellow circle marks the ANSS catalog location (latitude: 40.28, longitude: -124.39); green circle marks Elarms calculated location. Seismic stations used for solving the event parameters are marked as green triangles, while other stations are marked as blue triangles. The blind zone is marked as a red circle and the propagating S-wave front in increments of 1 s are marked as white circles.

length. Implementing MAMA back projection in real time and incorporating that into EEWs (Meng et al. 2014) could improve estimates of earthquake magnitude and shaking intensity distribution based on finite-fault models rather than point-source models. Other methods for estimating rupture size through the finite-fault approach have been developed for EEWs using Global Navigation Satellite Systems stations (e.g., Allen and Ziv 2011, Crowell et al. 2016, Grapenthin et al. 2014, Minson et al. 2014) or dense seismic stations (e.g., Böse et al. 2015). Using a MAMA deployed around an existing seismic station will allow a cost-effective augmentation of the station as well as enable finite-fault-based EEWs in remote areas with sparse stations or no GPS measurements.

Finally, the redundant data of the MAMA can also be used to eliminate false triggers and compute more robust event classifications, thus mitigating false alerts more common at the edge of the seismic network (Chung et al. 2016). The robustness and rapidity of the solutions obtained using MAMA can significantly improve warning times for natural hazards such as earthquakes and tsunamis, providing better estimation of source parameters and expected ground shaking (Melgar et al. 2016).

CONCLUSIONS

We have discussed the potential benefits of using MAMA in EEWs and seismological research. By exploiting array processing approaches, cost-effective MAMA can be used for

faster, more reliable earthquake location solutions, fault trace dimension estimation, and rupture propagation characterization as well as to support EEWS networks, particularly around the edges of networks and in sparsely instrumented regions. MAMA nodes can augment an existing seismic station or be used as an additional lower-quality station to densify a seismic network (e.g., Wu 2015). The limited resources needed to install a MAMA node also make it appealing for fast deployment and crisis response.

We have shown examples of the usefulness of MAMA by calculating the BAZ for several earthquakes using our new MAMA nodes. We have described a prototype of a MEMS DAU, which includes telemetry capabilities and a data logger with a limited production cost of less than U.S. \$150, which can be further lowered by mass production. Though the device is still under development, initial results and noise measurements show it can theoretically detect Mw 2.5 and larger events at 10 km and Mw 4.5 and larger at 100 km (Figure 2) using a frequency band of 1–10 Hz. Using nine-node MAMAs, currently deployed at the University of California Berkeley and at the Humboldt State University campuses, we demonstrate BAZ calculations of seven events ranging from Mw 2.7 to Mw 5.1 and distances ranging from as near as 5 km to over 100 km. Future work will include improving MAMA nodes and deploying more MAMAs at various locations as well as implementing BAZ calculations in real time (e.g., Eisermann et al. 2018).

ACKNOWLEDGMENTS

Ran N. Nof was funded by a fellowship from the Geological Survey of Israel (GSI), at the Ministry of Energy and Water Resources, and the project was supported by the United States–Israel Binational Science Foundation and the Raymond and Beverly Sackler Fund for Convergence Research in Biomedical, Physical and Engineering Sciences. The authors would like to thank the Berkeley Seismology Lab Technicians, George Dorian and Zack Alexy, and Oren Huber, Soenke Moeller, Eli Megidish, Andy Morrish, and Anatoli Mordakhay for their tips and help with the MAMA Node PCB design. Figures in this paper were produced by Python 2D plotting module Matplotlib (Hunter 2007) and ObsPy (Beyreuther et al. 2010). Background maps tiles are downloaded from ESRI world street map service: http://server.arcgisonline.com/ArcGIS/rest/services/Canvas/World_Light_Gray_Base/MapServer (last accessed August 5, 2017). Waveform data for this study are available upon request at the Northern California Earthquake Data Center (Stations names are BK.BRKXX..HN? and BK.ARCXX..HN?, where XX is in the range of 01–12 and 20–33 for the BRK and ARC MAMAs, respectively; the “?” may be replaced by E, N, or Z for channel orientation). We would like to thank the editor, Jonathan P. Stewart, the Associate editor, Antonino D’Alessandro, and two other anonymous reviewers for their comments and suggestions to improve this manuscript.

APPENDICES

Please refer to the online version of this manuscript to access the supplementary material provided in Appendices A and B.

REFERENCES

- Allen, R. M., and Ziv, A., 2011. Application of real-time GPS to earthquake early warning, *Geophysical Research Letters* **38**, 1–7.

- Allmann, B. P., and Shearer, P. M., 2007. Spatial and temporal stress drop variations in small earthquakes near Parkfield, California, *Journal of Geophysical Research: Solid Earth* **112**, 1–17.
- Advanced National Seismic System Technical Integration Committee Working Group on Instrumentation, Siting, Installation, and Site Metadata, 2008. *Instrumentation Guidelines for the Advanced National Seismic System, Report 2008-1262*, U.S. Geological Survey Reston, VA.
- Bartlett, M. S., 1950. Periodogram analysis and continuous spectra, *Biometrika* **37**, 1–16.
- Beyreuther, M., Barsch, R., Krischer, L., Megies, T., Behr, Y., and Wassermann, J., 2010. ObsPy: A Python toolbox for seismology, *Seismological Research Letters* **81**, 530–533.
- Birtill, J. W., and Whiteway, F. E., 1965. The application of phased arrays to the analysis of seismic body waves, *Philosophical Transactions of the Royal Society A: Mathematical, Physical and Engineering Sciences* **258**, 421–493.
- Böse, M., Felizardo, C., and Heaton, T. H., 2015. Finite-Fault Rupture Detector (FinDer): going real-time in Californian ShakeAlert Warning System, *Seismological Research Letters* **86**, 1692–1704.
- Cauzzi, C., and Clinton, J., 2013. A high- and low-noise model for high-quality strong-motion accelerometer stations, *Earthquake Spectra* **29**, 85–102.
- Chung, A. I., Allen, R. M., Henson, I., Hellweg, M., and Neuhauser, D., 2016. ElarmS 2015 performance and new Filterbank Teleseismic Filter, in *Seismological Society of America Annual Meeting*, 20–22 April, 2016, Reno, NV.
- Chung, A. I., Neighbors, C., Belmonte, A., Miller, M., Sepulveda, H. H., Christensen, C., Jakka, R. S., Cochran, E. S., and Lawrence, J., 2011. The Quake-Catcher Network Rapid Aftershock Mobilization Program following the 2010 M 8.8 Maule, Chile Earthquake, *Seismological Research Letters* **82**, 526–532.
- Clayton, R. W., Heaton, T., Chandy, M., Krause, A., Kohler, M., Bunn, J., Guy, R., Olson, M., Faulkner, M., Cheng, M., Strand, L., Chandy, R., Obenshain, D., Liu, A., and Aivazis, M., 2011. Community seismic network, *Annals of Geophysics* **54**, 738–747.
- Clayton, R. W., Heaton, T., Kohler, M., Chandy, M., Guy, R., and Bunn, J., 2015. Community Seismic Network: a dense array to sense earthquake strong motion, *Seismological Research Letters* **86**, 1–10.
- Clinton, J. F., and Heaton, T. H., 2002. Potential advantages of a strong-motion velocity meter over a strong-motion accelerometer, *Seismological Research Letters* **73**, 332–342.
- Cochran, E., Lawrence, J., Christensen, C., and Chung, A., 2009. A novel strong-motion seismic network for community participation in earthquake monitoring, *IEEE Instrumentation and Measurement Magazine* **12**, 8–15.
- Crowell, B. W., Schmidt, D. A., Bodin, P., Vidale, J. E., Gombert, J., Renate Hartog, J., Kress, V. C., Melbourne, T. I., Santillan, M., Minson, S. E., and Jamison, D. G., 2016. Demonstration of the Cascadia G-FAST Geodetic Earthquake Early Warning System for the Nisqually, Washington, Earthquake, *Seismological Research Letters* **87**, 930–943.
- D'Alessandro, A., 2014. Monitoring of earthquakes using MEMS sensors, *Current Science* **107**, 733–734.
- D'Alessandro, A., and D'Anna, G., 2013. Suitability of low-cost three-axis MEMS accelerometers in strong-motion seismology: tests on the LIS331DLH (iPhone) accelerometer, *Bulletin of the Seismological Society of America* **103**, 2906–2913.
- Eisermann, A. S., Ziv, A., and Wust-Bloch, H. G., 2018. Array-based earthquake location for regional earthquake early warning: case studies from the Dead Sea Transform, *Bulletin of the Seismological Society of America* **108**, 2046–2053.

- Evans, J. R., Allen, R. M., Chung, A. I., Cochran, E. S., Guy, R., Hellweg, M., and Lawrence, J. F., 2014. Performance of several low-cost accelerometers, *Seismological Research Letters* **85**, 147–158.
- Field, E. H., Jordan, T. H., Page, M. T., Milner, K. R., Shaw, B. E., Dawson, T. E., Biasi, G., Parsons, T. E., Hardebeck, J. L., Michael, A. J., Weldon, R., Powers, P., Johnson, K. M., Zeng, Y., Bird, P., Felzer, K., van der Elst, N., Madden, C., Arrowsmith, R., Werner, M. J., and Thatcher, W. R., 2017. A synoptic view of the third uniform California Earthquake Rupture Forecast (UCERF3), *Seismological Research Letters* **88**, 1259–1267.
- Finazzi, F., 2016. The Earthquake Network Project: toward a crowdsourced smartphone-based earthquake early warning system, *Bulletin of the Seismological Society of America* **106**, 1088–1099.
- Fletcher, J. B., Spudich, P., and Baker, L. M., 2006. Rupture propagation of the 2004 Parkfield, California, earthquake from observations at the UPSAR, *Bulletin of the Seismological Society of America* **96**, S129–S142.
- Grapenthin, R., Johanson, I., and Allen, R. M., 2014. The 2014 Mw 6.0 Napa earthquake, California: observations from real-time GPS-enhanced earthquake early warning, *Geophysical Research Letters* **41**, 8269–8276.
- Harjes, H. P., and Henger, M., 1973. Array-Seismologie, *Zeitschrift für Geophysik* **39**, 865–905.
- Holland, A., 2003. Earthquake data recorded by the MEMS accelerometer: field testing in Idaho, *Seismological Research Letters* **74**, 20–26.
- Horiuchi, S., Horiuchi, Y., Yamamoto, S., Nakamura, H., Wu, C., Rydelek, P. A., and Kachi, M., 2009. Home seismometer for earthquake early warning, *Geophysical Research Letters* **36**, L00B04.
- Hunter, J. D., 2007. Matplotlib: A 2D graphics environment, *Computing in Science & Engineering* **9**, 90–95.
- Kong, Q., Allen, R. M., Schreier, L., and Kwon, Y. W., 2016. MyShake: a smartphone seismic network for earthquake early warning and beyond, *Science Advances* **2**, e1501055.
- Kuyuk, S. H., Allen, R. M., Brown, H., Hellweg, M., Henson, I., and Neuhauser, D., 2014. Designing a network-based earthquake early warning algorithm for California: ElarmS-2, *Bulletin of the Seismological Society of America* **104**, 162–173.
- Lawrence, J. F., Cochran, E. S., Chung, A., Kaiser, A., Christensen, C. M., Allen, R., Baker, J. W., Fry, B., Heaton, T., Kilb, D., Kohler, D., and Taufer, M., 2014. Rapid earthquake characterization using MEMS accelerometers and volunteer hosts following the M 7.2 Darfield, New Zealand, earthquake, *Bulletin of the Seismological Society of America* **104**, 184–192.
- McNamara, D. E., and Buland, R. P., 2004. Ambient noise levels in the Continental United States, *Bulletin of the Seismological Society of America* **94**, 1517–1527.
- Melgar, D., Allen, R. M., Riquelme, S., Geng, J., Bravo, F., Baez, J. C., Parra, H., Barrientos, S., Fang, P., Bock, Y., Bevis, M., Caccamise, D. J., II, Vigny, C., Moreno, M., and Smalley, R., Jr., 2016. Local tsunami warnings: perspectives from recent large events, *Geophysical Research Letters* **43**, 1109–1117.
- Meng, L., Allen, R. M., and Ampuero, J. P., 2014. Application of seismic array processing to earthquake early warning, *Bulletin of the Seismological Society of America* **104**, 2553–2561.
- Middlemiss, R. P., Samarelli, A., Paul, D. J., Hough, J., Rowan, S., and Hammond, G. D., 2016. Measurement of the earth tides with a MEMS gravimeter, *Nature* **531**, 614–617.

- Minson, S. E., Brooks, B. A., Glennie, C. L., Murray, J. R., Langbein, J. O., Owen, S. E., Heaton, T. H., Iannucci, R. A., and Hauser, D. L., 2015. Crowdsourced earthquake early warning, *Science Advances* **1**, e1500036.
- Minson, S. E., Murray, J. R., Langbein, J. O., and Gomberg, J. S., 2014. Real-time inversions for finite fault slip models and rupture geometry based on high-rate GPS data, *Journal of Geophysical Research: Solid Earth* **119**, 3201–3231.
- Nawab, S. H., Dowla, F. U., and Lacoss, R. T., 1985. Direction determination of wideband signals, *IEEE Transactions on Acoustics, Speech, and Signal Processing* **33**, 1114–1122.
- Peterson, J., 1993. *Observations and Modeling of Seismic Background Noise*, USGS Open File Report 93-322, U.S. Geological Survey, Reston, VA.
- Pike, W. T., Delahunty, A. K., Mukherjee, A., Dou, G., Liu, H., Calcutt, S., and Standley, I. M., 2014. A self-levelling nano-g silicon seismometer, in *Proceedings of IEEE SENSORS 2014*, 2–5 November, 2014, Valencia, Spain.
- Rost, S., and Thomas, C., 2002. Array seismology: methods and applications, *Reviews of geophysics* **40**, 1–2.
- Rost, S., and Thomas, C., 2009. Improving seismic resolution through array processing techniques, *Surveys in Geophysics* **30**, 271–299.
- Schweitzer, J., Fyen, J., Mykkeltveit, S., Gibbons, S. J., Pirli, M., Kühn, D., and Kvaerna, T., 2011. Seismic arrays, in *New Manual of Seismological Observatory Practice (NMSOP-2)* (P. Bormann, ed.), GFZ German Research Centre for Geosciences, Potsdam, Germany, 1–80.
- Spudich, P., and Cranswick, E., 1984. Direct observation of rupture propagation during the 1979 Imperial Valley Earthquake using a short baseline accelerometer array, *Bulletin of the Seismological Society of America* **74**, 2083–2114.
- Tu, R., Wang, R., Ge, M., Walter, T. R., Ramatschi, M., Milkereit, C., Bindi, D., and Dahm, T., 2013. Cost-effective monitoring of ground motion related to earthquakes, landslides, or volcanic activity by joint use of a single-frequency GPS and a MEMS accelerometer, *Geophysical Research Letters* **40**, 3825–3829.
- Wu, Y. M., 2015. Progress on development of an earthquake early warning system using low-cost sensors, *Pure and Applied Geophysics* **172**, 2343–2351.
- Yildirim, B., Cochran, E. S., Chung, A., Christensen, C. M., and Lawrence, J. F., 2015. On the reliability of Quake-Catcher Network Earthquake Detections, *Seismological Research Letters* **86**, 856–869.
- Zheng, H., Shi, G., Zeng, T., and Li, B., 2011. Wireless earthquake alarm design based on MEMS accelerometer, in *2011 IEEE International Conference on Consumer Electronics, Communications and Networks (CECNet)*, 16–18 April, 2011, XianNing, China.
- Zou, X., Thiruvankatanathan, P., and Seshia, A. A., 2014. A seismic-grade resonant MEMS accelerometer, *Journal of Microelectromechanical Systems* **23**, 768–770.

(Received 12 February 2018; Accepted 20 July 2018)